

Smog Chamber Study on the Role of NO_x in SOA and O₃ Formation from Aromatic Hydrocarbons

Tianzeng Chen, Peng Zhang, Qingxin Ma, Biwu Chu, Jun Liu, Yanli Ge, and Hong He*



Cite This: *Environ. Sci. Technol.* 2022, 56, 13654–13663



Read Online

ACCESS |



Metrics & More



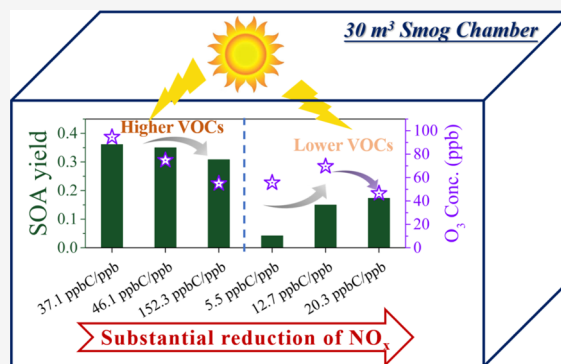
Article Recommendations



Supporting Information

ABSTRACT: China is facing dual pressures to reduce both PM_{2.5} and O₃ pollution, the crucial precursors of which are NO_x and VOCs. In our study, the role of NO_x in both secondary organic aerosol (SOA, the important constituent of PM_{2.5}) and O₃ formation was examined in our 30 m³ indoor smog chamber. As revealed in the present study, the NO_x level can obviously affect the OH concentration and volatility distribution of gas-phase oxidation products and thus O₃ and SOA formation. Reducing the NO_x concentration to the NO_x-sensitive regime can inhibit O₃ formation (by 42%), resulting in the reduction of oxidation capacity, which suppresses the SOA formation (by 45%) by inhibiting the formation of O- and N-containing gas-phase oxidation products with low volatility. The contribution of these oxidation products to the formation of SOA was also estimated, and the results could substantially support the trend of SOA yield with NO_x at different VOC levels. The atmospheric implications of NO_x in the coordinated control of PM_{2.5} and O₃ are also discussed.

KEYWORDS: ozone, secondary organic aerosol, NO_x concentration, aromatic hydrocarbons, gas-phase oxidation products



1. INTRODUCTION

In recent years, with the imposition of strict policies and control initiatives by the Chinese government, the air quality as characterized by PM_{2.5} (with less than 2.5 μm in aerodynamic diameter) has been greatly improved in China.¹ However, the annual mean PM_{2.5} concentration of 30 μg m⁻³ in China in 2021 (<http://106.37.208.233:20035/>) still far exceeds the guideline value (5 μg m⁻³) of the World Health Organization (WHO).^{1,2} Meanwhile, the O₃ concentration presents an increasing trend year by year, with the result that O₃ pollution has gradually attracted more attention.^{3,4} Therefore, China is facing a complex air pollution problem with high PM_{2.5} and O₃ levels coexisting that developed countries have not experienced, which highlights the urgency of coordinated control of PM_{2.5} and O₃ for China.

Nitrogen oxides (NO_x) and volatile organic compounds (VOCs) are essential precursors for the formation of O₃ and secondary organic aerosol (SOA), which are the important species in PM_{2.5}. NO_x can react with RO_x radicals (RO_x = OH + HO₂ + RO₂) to influence the RO_x cycle, thereby affecting the oxidation of VOCs and subsequent formation of O₃ and SOA.^{5,6} Meanwhile, the relative abundance of NO_x and VOCs has been proved to be important for determining O₃ and SOA concentrations.^{7–9} At low NO_x concentrations, which usually is referred to as the NO_x-limited regime, the formation of O₃ is primarily controlled by the reactions of HO₂ and RO₂ with NO, and the O₃ concentration can be almost linearly enhanced

by the increase of NO_x.¹⁰ At high NO_x concentrations, the increased NO_x concentration will promote the termination reaction of OH with NO₂, resulting in lower production of RO₂ and O₃. On the other hand, an increase in VOCs under high NO_x concentration conditions will cause an increase in RO₂ and thus O₃ production, which is defined as the VOC-limited regime.¹⁰ These two scenarios collectively illustrate the importance of the reaction of NO and RO₂ for the formation of O₃.¹¹ As for the role of NO_x in SOA formation, most chamber studies have indicated that the SOA yield will decrease as the NO_x concentration increases.^{12,13} This has generally been attributed to the competition between the reactions of NO_x + RO₂ and HO₂ + RO₂ under different NO_x levels, in which the latter will form more products with lower volatility to contribute to SOA formation and is predominant at low NO_x levels.^{14,15} NO_x could also affect SOA formation through changing OH levels via the reactions of OH + NO₂ → HNO₃ and HO₂ + NO → OH + NO₂.^{6,16,17} Meanwhile, previous studies demonstrated that the formation of organic nitrates (ONs, including RONO₂ and RO₂NO₂) becomes

Received: June 4, 2022

Revised: September 6, 2022

Accepted: September 7, 2022

Published: September 22, 2022



Table 1. Detailed Experimental Conditions in the Present Study

exp. no.	RH (%)	<i>T</i> (°C)	HC ₀ (ppb)	NO ₀ (ppb)	NO _{2,0} (ppb)	NO _{x,0} (ppb)	HC ₀ /NO _{x,0} (ppbC ppb ⁻¹)	ΔHC (ppb)	O ₃ (ppb)	ΔMo (μg m ⁻³)	SOA yield ^b	corrected SOA yield ^c
Tol01 ^a	5.0 ± 1	26 ± 1	14.6	18.4	0.2	18.6	5.5	6.2	55.6	0.01	0.001	0.042
Tol02	5.0 ± 1	26 ± 1	14.6	7.3	0.7	8.0	12.7	8.2	69.6	0.17	0.005	0.150
Tol03	5.0 ± 1	26 ± 1	14.6	2.5	0.3	2.8	37.1	7.9	46.5	0.35	0.011	0.173
Tol04	5.0 ± 1	26 ± 1	52.7	18.1	0.1	18.2	20.3	30.1	94.6	5.8	0.048	0.361
Tol05	5.0 ± 1	26 ± 1	52.7	5.8	2.2	8.0	46.1	23.4	74.8	4.7	0.047	0.357
Tol06	5.0 ± 1	26 ± 1	52.7	2.1	0.3	2.4	152.3	20.0	54.9	3.2	0.039	0.308

^aTol represents toluene. ^bSOA yield is equal to the mass concentration of corrected SOA divided by the consumed toluene. ^cSOA yield was corrected after considering the vapor and particle wall loss.

more important at high NO_x concentrations.^{6,18} Additionally, the availability of oxidants driving RO₂ formation rates will simultaneously decline with the decrease of NO_x, which will offset the increase in SOA formation caused by the enhancement of RO₂ autoxidation.¹⁹ Most recently, based on a self-developed novel integrated assessment system model, Ding et al.²⁰ indicated that NO_x emission reduction is essential to achieve the synergistic reduction of ambient PM_{2.5} and O₃ pollution, regardless of the reduction of VOC emission for the Beijing–Tianjin–Hebei regions. Many studies have also emphasized the importance of VOC reduction in urban areas.^{20–22} However, there is still a lack of systematic and quantitative experimental research on this topic. Additionally, there are still obvious gaps between observed and predicted concentrations of O₃ and SOA.^{23,24} These findings highlight the need to improve fundamental knowledge on the chemical pathways of O₃ and SOA evolution, especially NO_x-related processes under more atmospherically relevant conditions.

Aromatic hydrocarbons (such as toluene) are a class of anthropogenic VOCs (AVOCs) that are widely present in urban air^{25–27} and have a greater O₃ and SOA formation potential.^{25,28–30} Previous studies have been conducted to obtain the O₃ formation potential of individual AVOCs to support the development of O₃ control strategies.^{31,32} Meanwhile, their photo-oxidation mechanisms and SOA yields under different NO_x conditions have also been widely investigated.^{12,33–35} However, most of the studies focus only on the formation of O₃ or SOA and rarely on both.³⁶ There is currently a lack of research on the importance of NO_x and VOCs for both O₃ and SOA formation. Therefore, it is crucial to further understand the effect of NO_x on O₃ and SOA formation and evolution, and more quantitative studies on both aspects are continuously needed.

In this study, smog chamber experiments on the photo-oxidation of aromatics at various NO_x concentrations (2.4–18.6 ppb) were conducted to investigate the role of NO_x in O₃ and SOA formation. The formation of gas-phase oxidation products, especially the O- and N-containing products, as well as the chemical composition of SOA at different NO_x concentrations, was systematically analyzed and compared. Moreover, the relationship between O₃ and SOA formation related to the NO_x concentration was also elucidated. Finally, the atmospheric implications of NO_x in the coordinated control of PM_{2.5} and O₃ are also discussed.

2. EXPERIMENTAL METHODS

A series of photo-oxidation smog chamber experiments of toluene (Peking Reagent, 99.5%) and other aromatics were carried out under a series of different NO_x concentrations in our 30 m³ smog chamber that has been described in our

previous studies.^{37,38} To be brief, a cuboid Teflon reactor was placed in an indoor room, where the temperature (*T*) was mechanically controlled using an air conditioner system with an accuracy of ±1 °C. At the bottom of the reactor, a magnetic levitation fan coated with a Teflon film was used to mix the pollutants. One hundred and twenty UV lights (Philips TL 60/10R) with a peak intensity at 365 nm were installed in an array, and the light intensity characterized by the NO₂ photolysis rate (*J*_{NO₂}) was 0.55 min⁻¹, which can represent the light intensity at noon of Beijing.³⁹

Before the experiments, the purified zero air at a flow rate of 100 L min⁻¹ was used to clean the chamber until the concentration of residual contaminants is sufficiently low. And then, the liquid aromatic with a known volume was added into the chamber via Teflon piping carried by heated (~100 °C) zero air. The concentration of aromatics was measured by thermal desorption–gas chromatography–mass spectrometry (TD-GC/MS, Agilent). Subsequently, the desired NO_x concentration was introduced into the smog chamber using a mass flow controller from a standard gas cylinder (1020 ppm NO in N₂, Beijing Huayuan). And the concentration of NO_x was monitored in real time using a NO–NO₂–NO_x analyzer (model 42i-TL, Thermo). When the concentration of the reactants was basically stable, the UV lights were turned on to initiate the photochemical experiments. Each experiment was conducted at 26 ± 1 °C and 5.0 ± 1% relative humidity (RH) lasting for about 6 h, during which a temperature and relative humidity probe (Vaisala HMP110, Finland) were used to record *T* and RH with a time resolution of 1 min, respectively. Meanwhile, the gas-phase oxidation products were measured by an iodide high-resolution time-of-flight chemical-ionization mass spectrometer (HR-ToF-CIMS, ToFwerk AG, Aerodyne Research). The concentrations of formed O₃ and SOA were measured using an O₃ analyzer (model 49i, Thermo) and a scanning mobility particle sizer (SMPS, model 3082, TSI), respectively. Meanwhile, the concentration and chemical composition of SOA were detected synchronously using a high-resolution time-of-flight aerosol mass spectrometer (HR-ToF-AMS, Aerodyne Research), and monodisperse and dried ammonium nitrate aerosols with 300 nm were used to calibrate its ionization efficiency (IE). According to the method reported by Gordon et al.,⁴⁰ HR-ToF-AMS results were compared and corrected with the results of SMPS to characterize the concentration of SOA (details can be seen in Section S1.)

The detailed experimental conditions are summarized in Table 1. All species concentrations were corrected after considering the corresponding wall loss. The wall loss rates of gaseous species and aerosols have been carefully characterized and reported by our previous studies.^{41,42}

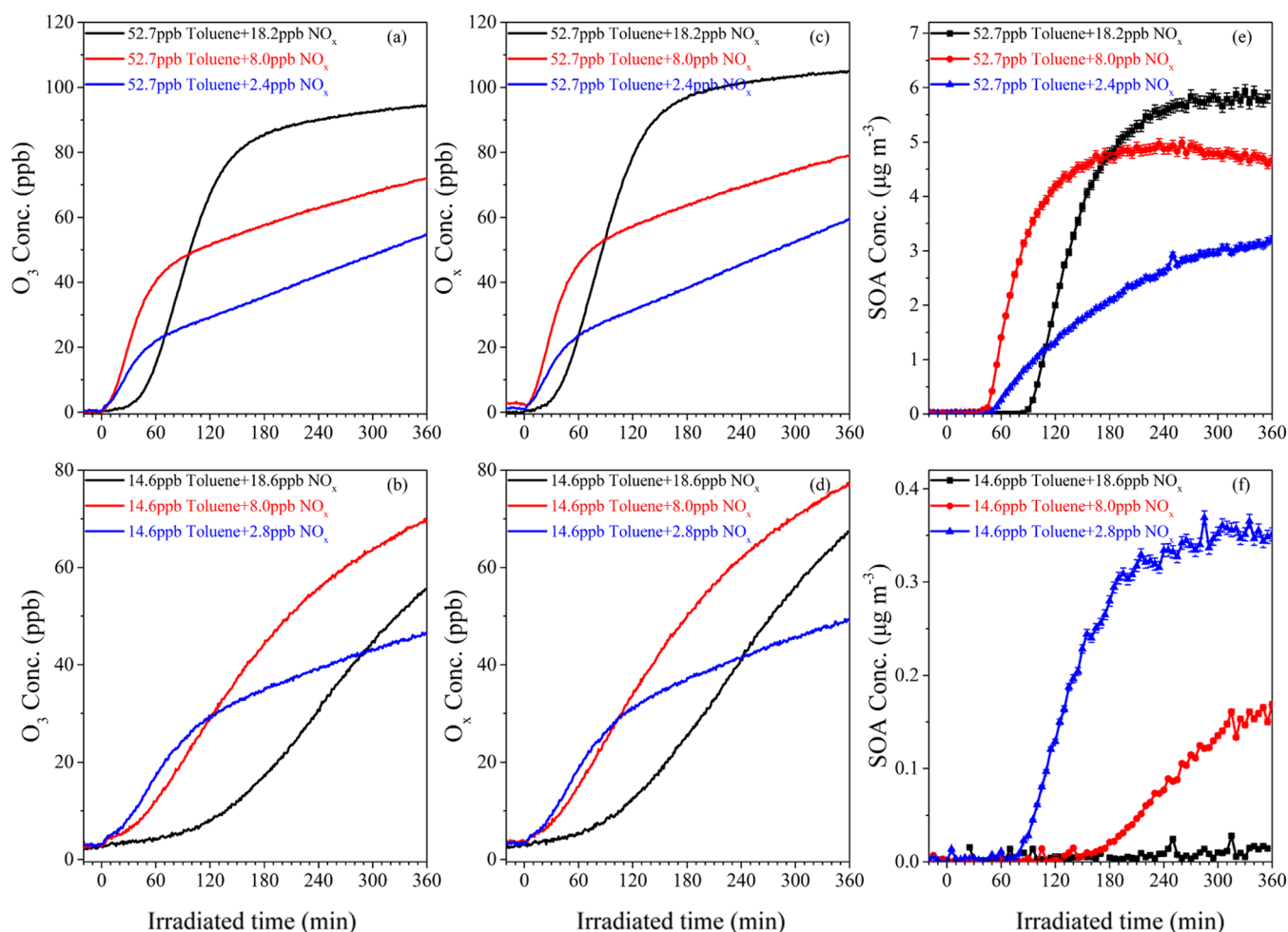


Figure 1. Time series of concentrations of (a, b) O₃, (c, d) O_x (=O₃ + NO₂), and (e, f) SOA generated in the photochemical reaction system of toluene with different NO_x concentrations (2.4–18.6 ppb) at two VOC concentration levels (52.7 and 14.6 ppb).

Importantly, the influence of vapor wall loss on SOA yield was carefully considered, and the detailed calculation process for the correction of SOA yield is given in Section S2. The corrected SOA yield as a function of NO_x still shows the same trend as we found.

3. RESULTS AND DISCUSSION

3.1. O₃ Formation under Different NO_x Conditions.

Figure 1 presents the evolution of O₃ and SOA concentrations formed in the photochemical reaction system of toluene with different concentrations of NO_x (2.4–18.6 ppb) at two VOC concentration levels. The higher VOC concentration level had higher ratios of VOCs/NO_x (20.3–152.3 ppbC ppb⁻¹) and was in the NO_x-sensitive regime. Hence, the reactions of NO with HO₂ and RO₂ determine the formation of O₃,^{10,43} resulting in a decrease in the concentration of O₃ formed after 360 min of the photochemical reaction by up to 42% as NO_x decreased (Table 1). However, the formation rate of O₃ at the initial stage of the reaction (0–30 min) showed a trend of first increasing and then decreasing as NO_x concentration decreased (Figure 2). This suggested that NO plays two aspect roles in the formation of O₃: one is the negative role of the chemical loss of O₃ caused by NO titration and another is the positive role of the reaction with RO₂ to form NO₂ and further to trigger the net accumulation of O₃. Meanwhile, both roles play a different dominated role under different levels of

NO conditions. At the highest NO concentration, the chemical loss of O₃ caused by NO titration dominates the loss of O₃, resulting in the lowest O₃ formation rate. At the lowest NO concentration, the contribution of the reaction of NO with RO₂ to form NO₂ and finally to O₃ was relatively weak, as well as the effect of NO titration, which combinedly lead to the moderate O₃ formation rate.

In contrast, at the lower VOC concentration level, the O₃ formation rate at the initial stage of the reaction (0–30 min) showed a trend of monotonically increasing as NO_x concentration decreased (Figure 2), which was related to the chemical loss of O₃ caused by NO titration. The O₃ concentration at the end of the reaction presented a tendency to first increase by 25% and then decrease by 33% as the NO_x concentration further decreased (Table 1), which was different from that under higher VOC conditions. The highest NO concentration level had a lower ratio of VOCs/NO_x (5.5 ppbC ppb⁻¹) and was in the VOC-sensitive regime. Under this condition, increased NO_x will reduce the OH concentration, which could also be supported by the estimated OH concentration as given in Figure S1, and then inhibit the formation of RO₂ and O₃,^{10,43} and vice versa. With further reduction of NO_x concentration to 2.8 ppb, the ratio of VOCs/NO_x increased to 37.1 ppbC ppb⁻¹, and the reaction system shifted to the NO_x-sensitive regime, resulting in the O₃ concentration decreased by 33% as NO_x decreased and

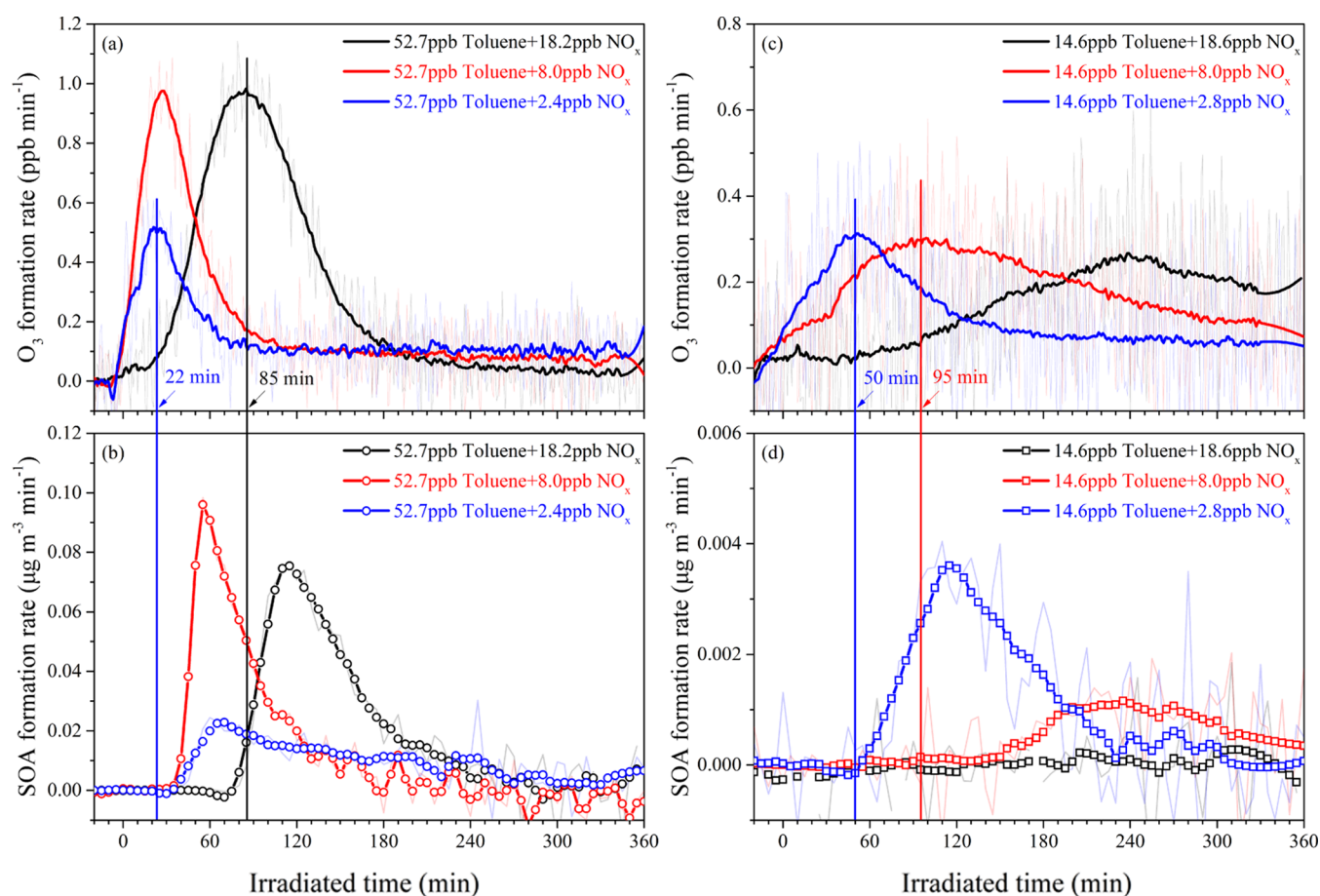


Figure 2. O₃ and SOA formation rate obtained from the photochemical reaction system of toluene with different NO_x concentrations (2.4–18.6 ppb) at two VOC concentration levels (52.7 and 14.6 ppb).

reaching the minimum O₃ concentration level (Table 1). Meanwhile, the trends of odd oxygen (O_x = NO₂ + O₃) production, which can reflect the oxidation capacity in the reaction systems, at both VOC concentration levels were consistent with the variation of O₃ concentration with NO_x (Figure 1). These results of O₃ concentration changing with the NO_x concentration implied that the deep control of NO_x to the NO_x-sensitive regime might be the effective way to reduce O₃ pollution in China.

Additionally, more experiments using mixed VOCs (including mixed aromatics, mixed toluene and long chain alkane, as well as mixed toluene and isoprene) were also conducted at similar NO_x concentration gradients, and the time-resolved results of O₃ and O_x concentrations are given in Figure S2. The changes in O₃ and O_x concentrations with the NO_x concentration using mixed VOCs are consistent with those obtained in the individual toluene system, and the detailed discussion can be seen in Section S3.

3.2. SOA Formation under Different NO_x Conditions.

As for SOA formation, the relatively high concentration of NO ([NO] ≫ [HO₂] + [RO₂]) in the initial stage resulted in the predominance of the reaction between RO₂ and NO to form alkoxy radicals, which are more volatile and uncondensable to SOA formation. As the reaction went on, NO was gradually converted to NO₂ and the [NO]/[NO₂] ratio decreased (Figure S3). Consequently, the reaction between RO₂ and HO₂ is dominant, resulting in more products with lower volatility that contribute to SOA formation.⁴⁴ The [NO]/

[NO₂] ratio corresponding to the time when SOA was just formed (defined as induction time) ranged from 0.17 to 0.30, which is roughly representative of [NO]/[NO₂] ratios (with an average of 0.22 ± 0.09) observed in Beijing, China.⁴⁵ Meanwhile, the induction time became shorter (80 vs 35 min, Figure 1) as NO_x decreased, which further supported the lower volatility of the products generated under low NO_x conditions.

Under higher VOC concentration conditions, the SOA concentration formed at the end of the reaction and SOA yield decreased with decreasing NO_x (Table 1), which might be related to the decreasing oxidation capacity in the reaction system. Similar NO_x dependencies of SOA yield have also been reported by previous studies.^{44,46} This could be supported by the decreasing estimated OH concentration as NO_x decreased (Figure S1). Higher OH concentration will promote the generation of low volatile oxidation products and thus SOA formation. Meanwhile, a higher concentration of SOA formation is always accompanied by the generation of higher O₃ concentrations with the change in NO_x, as shown in Figure 1. This implied that the increased O₃ can improve the oxidation capacity characterized by O_x in the reaction system, which will in turn facilitate the formation of SOA.^{47,48}

Contrastingly, under lower VOC concentration conditions, the SOA concentration was extremely low (0.01–0.35 μg m⁻³), with the corrected SOA yields of 4.2–17.3% (Table 1). These are comparable to the toluene SOA yield of 8.3% at 10 μg m⁻³ reported by Ng et al.¹² and relatively lower than those (~0.2–0.5) obtained by Zhang et al.⁴⁹ at the higher SOA

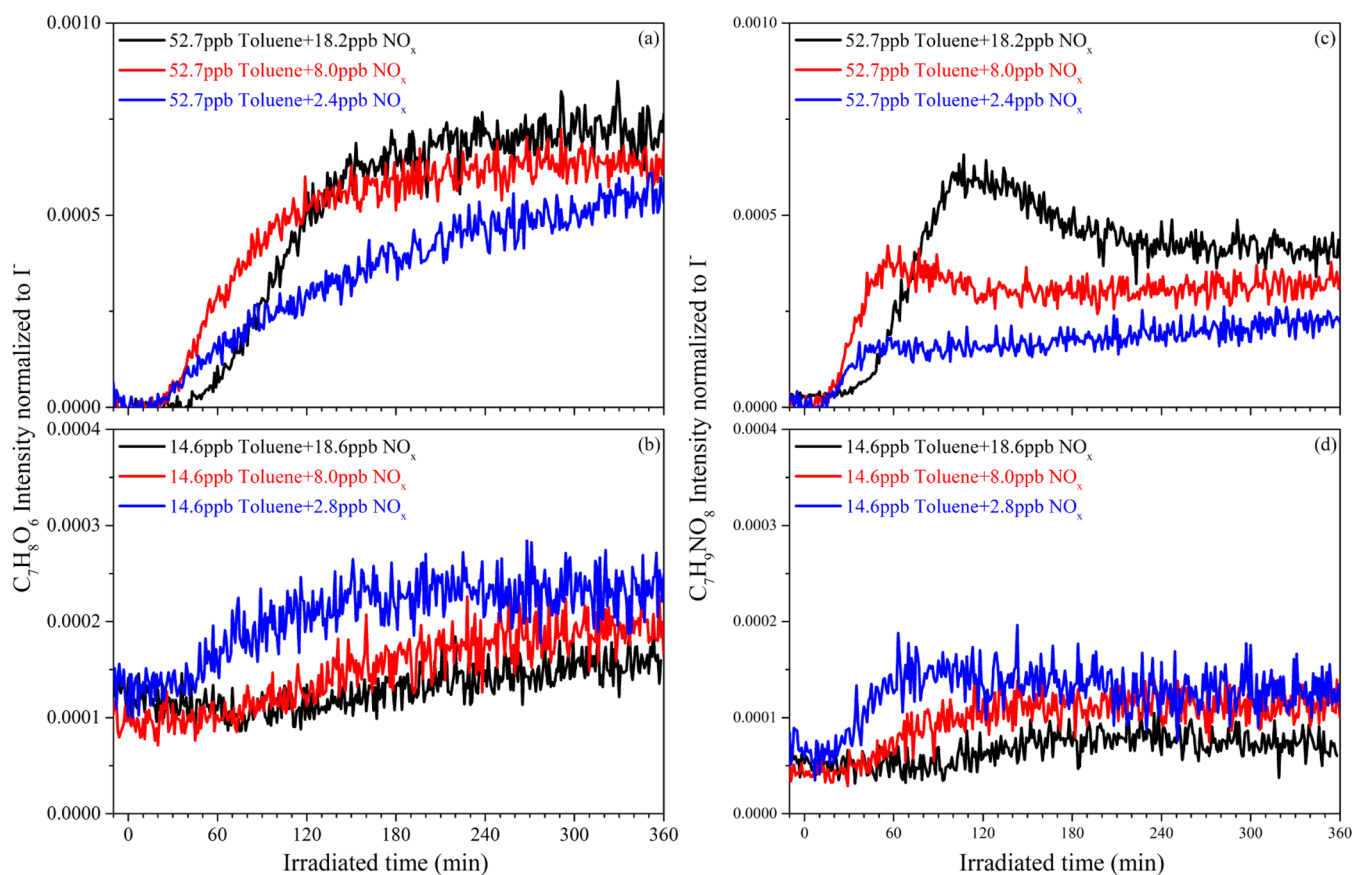


Figure 3. Time series of normalized intensities of (a, b) $C_7H_8O_6$ and (c, d) $C_7H_9NO_8$ generated in the photochemical reaction system of toluene with different NO_x concentrations (2.4–18.6 ppb) at two VOC concentration levels (52.7 and 14.6 ppb).

concentrations ($>20 \mu\text{g m}^{-3}$). The latter was associated with the higher concentrations of SOA available for gas-particle partitioning.³³ Meanwhile, increasing trends of SOA concentration and SOA yield were observed as NO_x decreased (Table 1). This was related to the enhanced branching ratio of RO_2 in reaction with HO_2 , which will form a hydroperoxide with low volatility, resulting in the enhancement of SOA via gas-particle partitioning.⁵⁰ Additionally, with the increase of O_x beyond a certain threshold, SOA increased synchronously with a regression slope ranging from 0.081 ± 0.002 to $0.163 \pm 0.002 \mu\text{g m}^{-3} \text{ppb}^{-1}$ (Figure S4), which was comparable with those observed in suburban Beijing ($0.130 \pm 0.002 \mu\text{g m}^{-3} \text{ppb}^{-1}$) by Chen et al.⁴⁵ and Mexico City ($0.160 \mu\text{g m}^{-3} \text{ppb}^{-1}$) by Wood et al.⁵¹ This implied that both secondary pollutants have some commonalities in terms of source.

3.3. O_3 and SOA Formation in Relation to Gas-Phase Oxidation Products. Gas-phase oxidation products containing carbon (C), hydrogen (H), oxygen (O), and nitrogen (N) in the form of iodide adducts were identified by our HR-ToF-CIMS, which has been widely reported to be sensitive to these species.^{52,53} The mass defect plot of these products is shown in Figure S5, which are classified into five categories, according to their saturation vapor concentration (C^*), i.e., oxidation products with volatility, intermediate volatility, semivolatility, low volatility, and extremely low volatility, abbreviated as VOC, IVOC, SVOC, LVOC, and ELVOC, respectively. According to these detected products, a detailed gas-phase chemical mechanism for photo-oxidation of toluene in the presence of NO_x was proposed as shown in Figure S6.

During the photochemical reaction of toluene with NO_x , the reaction of peroxy radicals (RO_2 and HO_2) with NO to produce NO_2 will result in net formation of O_3 . At the higher level of VOC concentration, the evolution of O_3 correlated closely with the evolution of N-containing gas-phase organics (e.g., $C_7H_9NO_8$, Figure 3) at the initial stage, which was related to the fact that both are directly or indirectly derived from the reaction of RO_2 and NO . As the reaction went on, the O_3 concentration continued to increase, while the N-containing gas-phase organics gradually decreased, which was related to the sinks of N-containing organics via gas-particle partitioning. The partitioning of these gas-phase oxidation products with low volatility formed in the photochemical reaction system determines the SOA formation.⁵⁰ Taking the highest multiple OH addition product as an example (Figure 3a), the concentration of $C_7H_8O_6$ formed at the end of the reaction decreased with decreasing NO_x , which was in line with the trend of OH with the NO_x level (Figure S1). Meanwhile, the corresponding N-containing organics ($C_7H_9NO_8$) also presented a similar decreasing trend as NO_x decreased (Figure 3c). Therefore, the trend of SOA tracked well with these low-volatility organic products and presented a decreasing trend as NO_x decreased (Figure 1). The higher OH concentration also caused a larger oxidation state ($OSc = 0.41 \pm 0.01$) of SOA generated at a higher NO_x concentration compared to that at a lower NO_x concentration ($OSc = 0.33 \pm 0.07$), during which OSc is equal to $2 \times O/C - H/C$, and H/C and O/C were derived from HR-ToF-AMS.⁵⁴

At the lower VOC concentration level, the concentration of O_3 at the end of the reaction was also positively correlated with

the normalized intensity of N-containing gas-phase organics (i.e., CHON organics) under different NO_x conditions (Figure S7). Meanwhile, the higher SOA concentration and yield were observed at a lower NO_x concentration (Table 1). This could be supported by the trend of bicyclic hydroperoxide ($\text{C}_7\text{H}_{10}\text{O}_5$), which is the reaction product of peroxide bicyclic peroxy radicals (BPRs), one type of RO_2 , with HO_2 . The yield of $\text{C}_7\text{H}_{10}\text{O}_5$ presented an increasing trend as NO_x decreased (Figure S8). Meanwhile, the concentration of $\text{C}_7\text{H}_8\text{O}_6$ and the corresponding N-containing organics ($\text{C}_7\text{H}_9\text{NO}_8$) also showed a similar increasing trend as NO_x decreased (Figure 3). In addition, as demonstrated by recent studies, the highly oxygenated organic molecules (HOMs) formed via RO_2 autoxidation might be enhanced with the decrease in NO_x .^{55–58} The partitioning of these gas-phase oxidation products to particle phase will contribute to SOA formation, resulting in an increasing trend of SOA yield as NO_x decreased under lower VOC concentration conditions (i.e., 14.6 ppb). However, this VOC concentration level is not easily achieved at the current stage due to the wealth of sources of VOCs and the lack of mature and effective control technology.

Comparing the SOA yield results obtained at different VOC concentration levels, it can be found that the effect of NO_x on SOA formation largely depends on the OH levels of the reaction systems (Figure S9). The change of SOA yield with NO_x is always consistent with the OH concentration. Overall, with the increase of VOCs/NO_x , the SOA yield and OH concentration both first increased and then decreased. This was related to the increase in VOC/NO_x , resulting in a change under reaction conditions from high NO_x to low NO_x . At very high NO_x concentrations, NO_x is acting as a sink for OH due to the reaction of $\text{OH} + \text{NO}_2 \rightarrow \text{HNO}_3$. The role of this OH sink weakened as the NO_x concentration decreased. With the continuous reduction of NO_x concentration to low NO_x condition, the recycling of OH through the reaction of $\text{HO}_2 + \text{NO} \rightarrow \text{OH} + \text{NO}_2$ was weakened. Similar NO_x dependencies of SOA formation have been reported by Sarrafzadeh et al.¹⁶ The level of OH determines the formation of gas-phase oxidation products, which in turn affects SOA generation via their partitioning. The seemingly contradictory trend of SOA yield with NO_x is essentially dominated by the gas-particle partitioning of these gas-phase oxidation products with low volatility. The volatility distributions of these products detected by HR-ToF-CIMS were estimated using the method mentioned by Bianchi et al.⁵⁷ (details can be seen in Section S4) and presented in Figure 4, which can support the aforementioned conclusions. As shown in Figure 4, the trends of the intensities of IVOC, SVOC, and LVOC with the NO_x concentration were all consistent with the trend of SOA yield, and there was a positive correlation between the intensity of these low-volatility organics and the SOA yield.

Furthermore, the contributions of these identified gas-phase oxidation products to SOA formation were quantitatively estimated (details can be seen in Section S5). It can be found that the gas-phase oxidation products belonging to the SVOC and LVOC categories are the dominant species to SOA formation under different photochemical reaction systems (Figure 5). The evolutions of the estimated SOA concentration with NO_x concentration further supported the trend of SOA yield with NO_x . Meanwhile, the estimated SOA using these oxidation products can explain the averaged 26.6–41.1% of SOA formation, where the percentage is the ratio between the estimated and measured SOA concentration. A recent

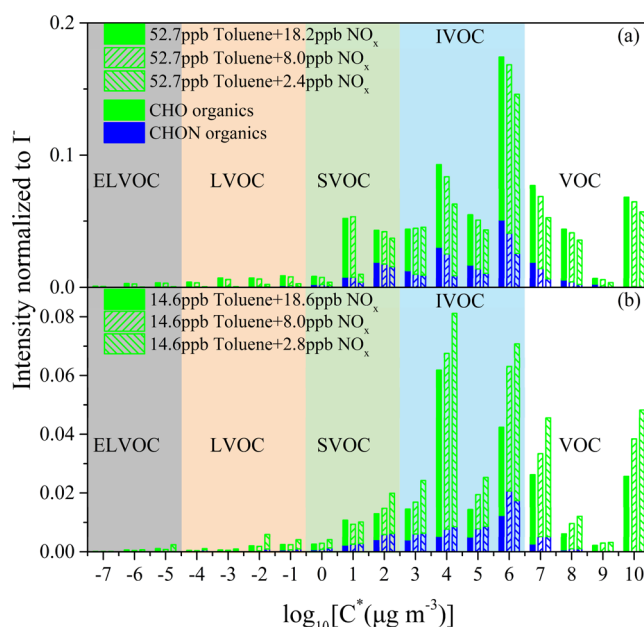


Figure 4. Volatility distributions of gas-phase oxidation products generated in the photochemical reaction system of toluene with different NO_x concentrations (2.4–18.6 ppb) at two VOC concentration levels (52.7 and 14.6 ppb). The normalized intensity to the ion source iodide was used.

study also reported similar proportions (26–39%) to explain the mass growth of organic aerosols through the condensation of the measured oxygenated organics.⁵⁹ Therefore, more instruments that can simultaneously obtain information on the molecular level of organic aerosols are urgently needed to be developed. Additionally, the evolution trend of N-containing organics with the level of NO_x is also consistent with the trend of SOA yield with NO_x (Figure S10). The concentration of N-containing compounds (NOCs) in the particle phase estimated using the $\text{NO}^+/\text{NO}_2^+$ ratio derived from HR-ToF-AMS⁶⁰ (details can be seen in the Section S6) could also support this phenomenon. It can be seen that the evolution trend of N-containing organics detected by HR-ToF-CIMS is positively related to the NOCs concentration (Figure S10). This suggests that N-containing organics formed in the photochemical reaction system of toluene with NO_x play an important role in SOA formation.

4. ATMOSPHERIC IMPLICATIONS

As revealed in the present study, reducing NO_x can result in the simultaneous reduction of O_3 and SOA formation at the higher VOC concentration, which can basically reflect the level of pollutants during polluted periods in China from the perspective of total OH reactivity.^{61,62} Under lower VOC concentration conditions, the O_3 concentration showed a trend of first increasing and then decreasing with further reduction of the NO_x concentration. These were related to the change of OH concentration and volatility distribution of gas-phase oxidation products with NO_x . Our laboratory study reveals the intrinsic mechanism of NO_x in influencing photochemical reactions to form O_3 and SOA, confirming the central role of NO_x in atmospheric oxidation capacity.

Many previous studies have demonstrated that NO_x can also contribute to the formation of nitrate and ammonium as well as play a key role in sulfate formation,^{37,63–65} which are the

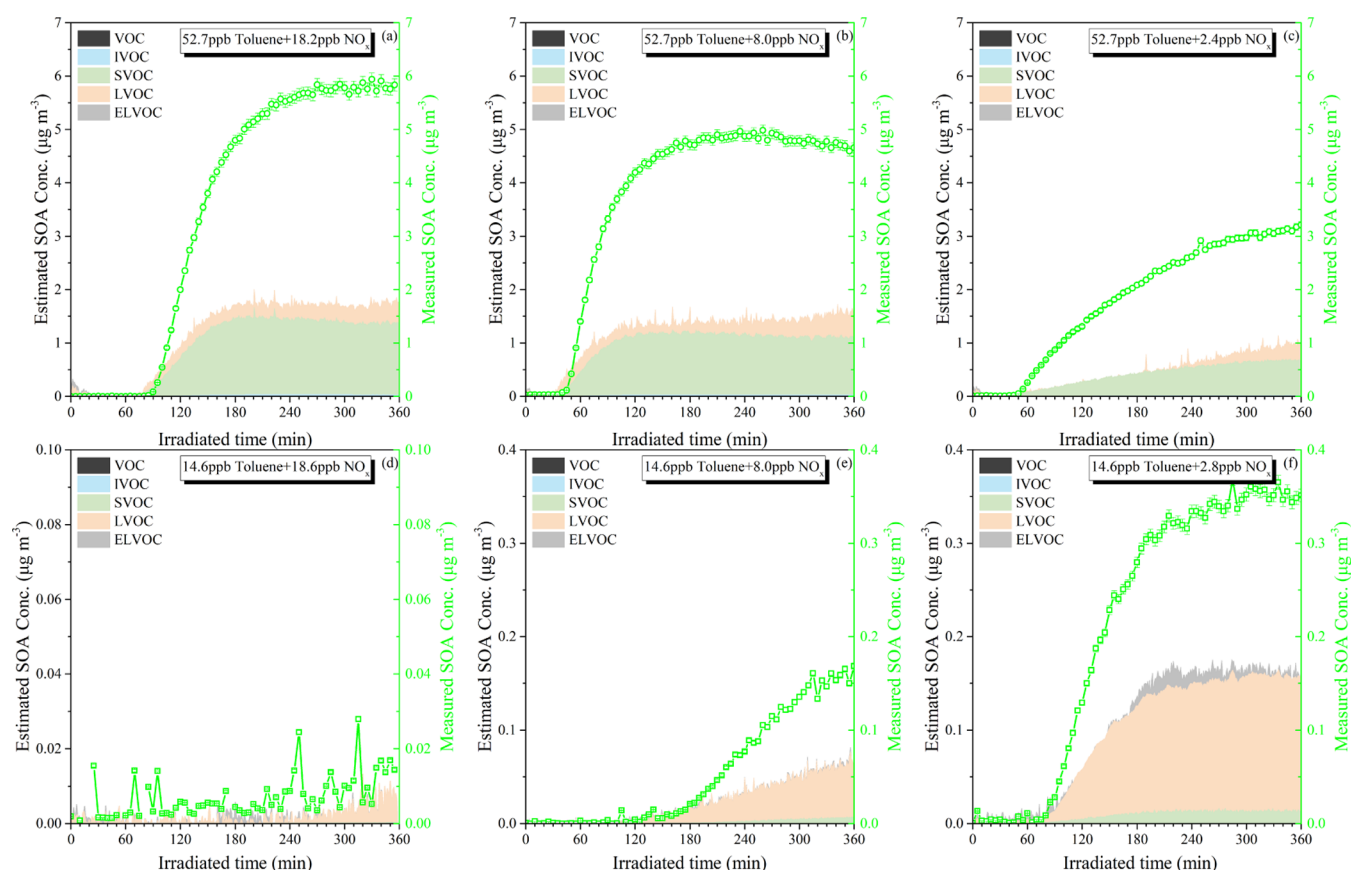


Figure 5. Time series of estimated (left y axis) and measured SOA concentration (right y axis) under different NO_x conditions (2.4–18.6 ppb) at two VOC concentration levels (52.7 and 14.6 ppb).

main inorganic components of $\text{PM}_{2.5}$. Our previous study also suggested that $\text{PM}_{2.5}$ concentrations were more sensitive to changes in NO_x than other gaseous pollutants.⁶⁶ As China is facing dual pressures to reduce both $\text{PM}_{2.5}$ and O_3 pollution, recent observations and modeling studies have suggested that the substantial reduction of NO_x is a feasible path to achieve coordinated control of both.^{20,67} Our laboratory study provides new evidence and scientific basis for this perspective.

ASSOCIATED CONTENT

Supporting Information

The Supporting Information is available free of charge at <https://pubs.acs.org/doi/10.1021/acs.est.2c04022>.

Detailed information on the AMS corrections; vapor wall loss corrections; O_3 and SOA formation in the mixed VOCs systems, as well as the method to obtain the volatility distributions of these gas-phase oxidation products, and their contribution to SOA formation; and method to estimate N-containing compounds (NOCs), and Figures S1–S10 were also included (PDF)

AUTHOR INFORMATION

Corresponding Author

Hong He – State Key Joint Laboratory of Environment Simulation and Pollution Control, Research Center for Eco-Environmental Sciences, Chinese Academy of Sciences, Beijing 100085, China; Center for Excellence in Regional Atmospheric Environment, Institute of Urban Environment, Chinese Academy of Sciences, Xiamen 361021, China;

University of Chinese Academy of Sciences, Beijing 100049, China; orcid.org/0000-0001-8476-8217; Email: honghe@rcees.ac.cn

Authors

Tianzeng Chen – State Key Joint Laboratory of Environment Simulation and Pollution Control, Research Center for Eco-Environmental Sciences, Chinese Academy of Sciences, Beijing 100085, China; orcid.org/0000-0001-8123-0534

Peng Zhang – State Key Joint Laboratory of Environment Simulation and Pollution Control, Research Center for Eco-Environmental Sciences, Chinese Academy of Sciences, Beijing 100085, China; University of Chinese Academy of Sciences, Beijing 100049, China; orcid.org/0000-0002-0620-7673

Qingxin Ma – State Key Joint Laboratory of Environment Simulation and Pollution Control, Research Center for Eco-Environmental Sciences, Chinese Academy of Sciences, Beijing 100085, China; Center for Excellence in Regional Atmospheric Environment, Institute of Urban Environment, Chinese Academy of Sciences, Xiamen 361021, China; University of Chinese Academy of Sciences, Beijing 100049, China

Biwu Chu – State Key Joint Laboratory of Environment Simulation and Pollution Control, Research Center for Eco-Environmental Sciences, Chinese Academy of Sciences, Beijing 100085, China; Center for Excellence in Regional Atmospheric Environment, Institute of Urban Environment, Chinese Academy of Sciences, Xiamen 361021, China; University of Chinese Academy of Sciences, Beijing 100049, China; orcid.org/0000-0002-7548-5669

Jun Liu – State Key Joint Laboratory of Environment Simulation and Pollution Control, Research Center for Eco-Environmental Sciences, Chinese Academy of Sciences, Beijing 100085, China; University of Chinese Academy of Sciences, Beijing 100049, China; orcid.org/0000-0002-3065-799X

Yanli Ge – State Key Joint Laboratory of Environment Simulation and Pollution Control, Research Center for Eco-Environmental Sciences, Chinese Academy of Sciences, Beijing 100085, China; University of Chinese Academy of Sciences, Beijing 100049, China

Complete contact information is available at:
<https://pubs.acs.org/10.1021/acs.est.2c04022>

Notes

The authors declare no competing financial interest.

ACKNOWLEDGMENTS

This work was supported by the National Natural Science Foundation of China (22006152, 22188102, and 21876185), the Cultivating Project of Strategic Priority Research Program of Chinese Academy of Sciences (XDPB1901), and the Young Talent Project of the Center for Excellence in Regional Atmospheric Environment, CAS (CERAE201801). The authors would like to express gratitude to Chunshan Liu and his company Beijing Convenient Environmental Tech Co. Ltd. (<http://www.bjkwnt.com/>) for their support in setting up our smog chamber. They also thank Qingcai Feng for her help in editing our manuscript.

REFERENCES

- (1) Zhang, Q.; Zheng, Y.; Tong, D.; Shao, M.; Wang, S.; Zhang, Y.; Xu, X.; Wang, J.; He, H.; Liu, W.; Ding, Y.; Lei, Y.; Li, J.; Wang, Z.; Zhang, X.; Wang, Y.; Cheng, J.; Liu, Y.; Shi, Q.; Yan, L.; Geng, G.; Hong, C.; Li, M.; Liu, F.; Zheng, B.; Cao, J.; Ding, A.; Gao, J.; Fu, Q.; Huo, J.; Liu, B.; Liu, Z.; Yang, F.; He, K.; Hao, J. Drivers of improved PM_{2.5} air quality in China from 2013 to 2017. *Proc. Natl. Acad. Sci. U.S.A.* **2019**, *116*, 24463–24469.
- (2) World Health Organization. *WHO Global Air Quality Guidelines: Particulate Matter (PM_{2.5} and PM₁₀), Ozone, Nitrogen Dioxide, Sulfur Dioxide and Carbon Monoxide*; World Health Organization: Geneva, 2021.
- (3) Wang, T.; Xue, L.; Brimblecombe, P.; Lam, Y. F.; Li, L.; Zhang, L. Ozone pollution in China: A review of concentrations, meteorological influences, chemical precursors, and effects. *Sci. Total Environ.* **2017**, *575*, 1582–1596.
- (4) Li, K.; Jacob, D. J.; Liao, H.; Qiu, Y.; Shen, L.; Zhai, S.; Bates, K. H.; Sulprizio, M. P.; Song, S.; Lu, X.; Zhang, Q.; Zheng, B.; Zhang, Y.; Zhang, J.; Lee, H. C.; Kuk, S. K. Ozone pollution in the North China Plain spreading into the late-winter haze season. *Proc. Natl. Acad. Sci. U.S.A.* **2021**, *118*, No. e2015797118.
- (5) Pusede, S. E.; Steiner, A. L.; Cohen, R. C. Temperature and Recent Trends in the Chemistry of Continental Surface Ozone. *Chem. Rev.* **2015**, *115*, 3898–3918.
- (6) Pullinen, I.; Schmitt, S.; Kang, S.; Sarrafzadeh, M.; Schlag, P.; Andres, S.; Kleist, E.; Mentel, T. F.; Rohrer, F.; Springer, M.; Tillmann, R.; Wildt, J.; Wu, C.; Zhao, D.; Wahner, A.; Kiendler-Scharr, A. Impact of NO_x on secondary organic aerosol (SOA) formation from α -pinene and β -pinene photooxidation: the role of highly oxygenated organic nitrates. *Atmos. Chem. Phys.* **2020**, *20*, 10125–10147.
- (7) Finlayson-Pitts, B. J.; Pitts, J. N. Chemistry of the Upper and Lower Atmosphere. In *Chemistry of the Upper and Lower Atmosphere*; Finlayson-Pitts, B. J., Pitts, J. N., Eds.; Academic Press: San Diego, 2000.
- (8) Seinfeld, J. H.; Pandis, S. N. *Atmospheric Chemistry and Physics: From Air Pollution to Climate Change*; John Wiley & Sons: Hoboken, NJ, 2016.
- (9) Zhao, D.; Schmitt, S. H.; Wang, M.; Acir, I. H.; Tillmann, R.; Tan, Z.; Novelli, A.; Fuchs, H.; Pullinen, I.; Wegener, R.; Rohrer, F.; Wildt, J.; Kiendler-Scharr, A.; Wahner, A.; Mentel, T. F. Effects of NO_x and SO₂ on the secondary organic aerosol formation from photooxidation of α -pinene and limonene. *Atmos. Chem. Phys.* **2018**, *18*, 1611–1628.
- (10) Sillman, S. The relation between ozone, NO_x and hydrocarbons in urban and polluted rural environments. *Atmos. Environ.* **1999**, *33*, 1821–1845.
- (11) Thornton, J. A.; Wooldridge, P. J.; Cohen, R. C.; Martinez, M.; Harder, H.; Brune, W. H.; Williams, E. J.; Roberts, J. M.; Fehsenfeld, F. C.; Hall, S. R.; Shetter, R. E.; Wert, B. P.; Fried, A. Ozone production rates as a function of NO_x abundances and HO_x production rates in the Nashville urban plume. *J. Geophys. Res.: Atmos.* **2002**, *107*, No. 4146.
- (12) Ng, N. L.; Kroll, J. H.; Chan, A. W. H.; Chhabra, P. S.; Flagan, R. C.; Seinfeld, J. H. Secondary organic aerosol formation from m-xylene, toluene, and benzene. *Atmos. Chem. Phys.* **2007**, *7*, 3909–3922.
- (13) Song, C.; Na, K.; Warren, B.; Malloy, Q.; Cocker, D. R. Secondary organic aerosol formation from m-xylene in the absence of NO_x. *Environ. Sci. Technol.* **2007**, *41*, 7409–7416.
- (14) Xu, J.; Griffin, R. J.; Liu, Y.; Nakao, S.; Cocker, D. R. Simulated impact of NO_x on SOA formation from oxidation of toluene and m-xylene. *Atmos. Environ.* **2015**, *101*, 217–225.
- (15) Lane, T. E.; Donahue, N. M.; Pandis, S. N. Effect of NO_x on Secondary Organic Aerosol Concentrations. *Environ. Sci. Technol.* **2008**, *42*, 6022–6027.
- (16) Sarrafzadeh, M.; Wildt, J.; Pullinen, I.; Springer, M.; Kleist, E.; Tillmann, R.; Schmitt, S. H.; Wu, C.; Mentel, T. F.; Zhao, D.; Hastie, D. R.; Kiendler-Scharr, A. Impact of NO_x and OH on secondary organic aerosol formation from β -pinene photooxidation. *Atmos. Chem. Phys.* **2016**, *16*, 11237–11248.
- (17) Li, L.; Tang, P.; Cocker, D. R. Instantaneous nitric oxide effect on secondary organic aerosol formation from m-xylene photo-oxidation. *Atmos. Environ.* **2015**, *119*, 144–155.
- (18) Lee, B. H.; Mohr, C.; Lopez-Hilfiker, F. D.; Lutz, A.; Hallquist, M.; Lee, L.; Romer, P.; Cohen, R. C.; Iyer, S.; Kurtén, T.; Hu, W.; Day, D. A.; Campuzano-Jost, P.; Jimenez, J. L.; Xu, L.; Ng, N. L.; Guo, H.; Weber, R. J.; Wild, R. J.; Brown, S. S.; Koss, A.; de Gouw, J.; Olson, K.; Goldstein, A. H.; Seco, R.; Kim, S.; McAvey, K.; Shepson, P. B.; Starn, T.; Baumann, K.; Edgerton, E. S.; Liu, J.; Shilling, J. E.; Miller, D. O.; Brune, W.; Schobesberger, S.; D'Ambro, E. L.; Thornton, J. A. Highly functionalized organic nitrates in the southeast United States: Contribution to secondary organic aerosol and reactive nitrogen budgets. *Proc. Natl. Acad. Sci. U.S.A.* **2016**, *113*, 1516–1521.
- (19) Pye, H. O. T.; D'Ambro, E. L.; Lee, B. H.; Schobesberger, S.; Takeuchi, M.; Zhao, Y.; Lopez-Hilfiker, F.; Liu, J.; Shilling, J. E.; Xing, J.; Mathur, R.; Middlebrook, A. M.; Liao, J.; Welti, A.; Graus, M.; Warneke, C.; de Gouw, J. A.; Holloway, J. S.; Ryerson, T. B.; Pollack, I. B.; Thornton, J. A. Anthropogenic enhancements to production of highly oxygenated molecules from autoxidation. *Proc. Natl. Acad. Sci. U.S.A.* **2019**, *116*, 6641–6646.
- (20) Ding, D.; Xing, J.; Wang, S.; Dong, Z.; Zhang, F.; Liu, S.; Hao, J. Optimization of a NO_x and VOC Cooperative Control Strategy Based on Clean Air Benefits. *Environ. Sci. Technol.* **2022**, *56*, 739–749.
- (21) Lyu, X.; Wang, N.; Guo, H.; Xue, L.; Jiang, F.; Zeren, Y.; Cheng, H.; Cai, Z.; Han, L.; Zhou, Y. Causes of a continuous summertime O₃ pollution event in Jinan, a central city in the North China Plain. *Atmos. Chem. Phys.* **2019**, *19*, 3025–3042.
- (22) Yang, G.; Liu, Y.; Li, X. Spatiotemporal distribution of ground-level ozone in China at a city level. *Sci. Rep.* **2020**, *10*, No. 7229.
- (23) Shrivastava, M.; Cappa, C. D.; Fan, J.; Goldstein, A. H.; Guenther, A. B.; Jimenez, J. L.; Kuang, C.; Laskin, A.; Martin, S. T.; Ng, N. L.; Petaja, T.; Pierce, J. R.; Rasch, P. J.; Roldin, P.; Seinfeld, J. H.; Shilling, J.; Smith, J. N.; Thornton, J. A.; Volkamer, R.; Wang, J.

Worsnop, D. R.; Zaveri, R. A.; Zelenyuk, A.; Zhang, Q. Recent advances in understanding secondary organic aerosol: Implications for global climate forcing. *Rev. Geophys.* **2017**, *55*, 509–559.

(24) Baier, B. C.; Brune, W. H.; Miller, D. O.; Blake, D.; Long, R.; Wisthaler, A.; Cantrell, C.; Fried, A.; Heikes, B.; Brown, S.; McDuffie, E.; Flocke, F.; Apel, E.; Kaser, L.; Weinheimer, A. Higher measured than modeled ozone production at increased NO_x levels in the Colorado Front Range. *Atmos. Chem. Phys.* **2017**, *17*, 11273–11292.

(25) Li, Q.; Su, G.; Li, C.; Liu, P.; Zhao, X.; Zhang, C.; Sun, X.; Mu, Y.; Wu, M.; Wang, Q.; Sun, B. An investigation into the role of VOCs in SOA and ozone production in Beijing, China. *Sci. Total Environ.* **2020**, *720*, No. 137536.

(26) Calvert, J. G.; Atkinson, R.; Becker, K. H.; Kamens, R. M.; Seinfeld, J. H.; Wallington, T. H.; Yarwood, G. *The Mechanisms of Atmospheric Oxidation of the Aromatic Hydrocarbons*; Oxford University Press: England, 2002.

(27) Zhang, Y.; Yang, W.; Simpson, I.; Huang, X.; Yu, J.; Huang, Z.; Wang, Z.; Zhang, Z.; Liu, D.; Huang, Z.; Wang, Y.; Pei, C.; Shao, M.; Blake, D. R.; Zheng, J.; Huang, Z.; Wang, X. Decadal changes in emissions of volatile organic compounds (VOCs) from on-road vehicles with intensified automobile pollution control: Case study in a busy urban tunnel in south China. *Environ. Pollut.* **2018**, *233*, 806–819.

(28) Wu, W.; Zhao, B.; Wang, S.; Hao, J. Ozone and secondary organic aerosol formation potential from anthropogenic volatile organic compounds emissions in China. *J. Environ. Sci.* **2017**, *53*, 224–237.

(29) Deng, W.; Liu, T.; Zhang, Y.; Situ, S.; Hu, Q.; He, Q.; Zhang, Z.; Lü, S.; Bi, X.; Wang, X.; Boreave, A.; George, C.; Ding, X.; Wang, X. Secondary organic aerosol formation from photo-oxidation of toluene with NO_x and SO₂: Chamber simulation with purified air versus urban ambient air as matrix. *Atmos. Environ.* **2017**, *150*, 67–76.

(30) Zhang, Y.; Wang, X.; Blake, D. R.; Li, L.; Zhang, Z.; Wang, S.; Guo, H.; Lee, F. S. C.; Gao, B.; Chan, L.; Wu, D.; Rowland, F. S. Aromatic hydrocarbons as ozone precursors before and after outbreak of the 2008 financial crisis in the Pearl River Delta region, south China. *J. Geophys. Res.: Atmos.* **2012**, *117*, No. D15306.

(31) Carter, W. P. L.; Pierce, J. A.; Luo, D.; Malkina, I. L. Environmental chamber study of maximum incremental reactivities of volatile organic compounds. *Atmos. Environ.* **1995**, *29*, 2499–2511.

(32) Carter, W. P. L. *Environmental Chamber Studies of Ozone Formation Potentials of Volatile Organic Compounds*; Springer Netherlands: Dordrecht, 2006; pp 231–240.

(33) Odum, J. R.; Hoffmann, T.; Bowman, F.; Collins, D.; Flagan, R. C.; Seinfeld, J. H. Gas/particle partitioning and secondary organic aerosol yields. *Environ. Sci. Technol.* **1996**, *30*, 2580–2585.

(34) Li, L.; Tang, P.; Nakao, S.; Chen, C. L.; Cocker, D. R., III Role of methyl group number on SOA formation from monocyclic aromatic hydrocarbons photooxidation under low-NO_x conditions. *Atmos. Chem. Phys.* **2016**, *16*, 2255–2272.

(35) Chen, T.; Liu, Y.; Chu, B.; Liu, C.; Liu, J.; Ge, Y.; Ma, Q.; Ma, J.; He, H. Differences of the oxidation process and secondary organic aerosol formation at low and high precursor concentrations. *J. Environ. Sci.* **2019**, *79*, 256–263.

(36) Luo, H.; Jia, L.; Wan, Q.; An, T.; Wang, Y. Role of liquid water in the formation of O₃ and SOA particles from 1,2,3-trimethylbenzene. *Atmos. Environ.* **2019**, *217*, No. 116955.

(37) Chen, T.; Chu, B.; Ge, Y.; Zhang, S.; Ma, Q.; He, H.; Li, S. M. Enhancement of aqueous sulfate formation by the coexistence of NO₂/NH₃ under high ionic strengths in aerosol water. *Environ. Pollut.* **2019**, *252*, 236–244.

(38) Chen, T.; Liu, Y.; Ma, Q.; Chu, B.; Zhang, P.; Liu, C.; Liu, J.; He, H. Significant source of secondary aerosol: formation from gasoline evaporative emissions in the presence of SO₂ and NH₃. *Atmos. Chem. Phys.* **2019**, *19*, 8063–8081.

(39) Chou, C. C. K.; Tsai, C. Y.; Chang, C. C.; Lin, P. H.; Liu, S. C.; Zhu, T. Photochemical production of ozone in Beijing during the 2008 Olympic Games. *Atmos. Chem. Phys.* **2011**, *11*, 9825–9837.

(40) Gordon, T. D.; Presto, A. A.; May, A. A.; Nguyen, N. T.; Lipsky, E. M.; Donahue, N. M.; Gutierrez, A.; Zhang, M.; Maddox, C.; Rieger, P.; Chattopadhyay, S.; Maldonado, H.; Maricq, M. M.; Robinson, A. L. Secondary organic aerosol formation exceeds primary particulate matter emissions for light-duty gasoline vehicles. *Atmos. Chem. Phys.* **2014**, *14*, 4661–4678.

(41) Chen, T.; Liu, Y.; Liu, C.; Liu, J.; Chu, B.; He, H. Important role of aromatic hydrocarbons in SOA formation from unburned gasoline vapor. *Atmos. Environ.* **2019**, *201*, 101–109.

(42) Chen, T.; Chu, B.; Ma, Q.; Zhang, P.; Liu, J.; He, H. Effect of relative humidity on SOA formation from aromatic hydrocarbons: Implications from the evolution of gas- and particle-phase species. *Sci. Total Environ.* **2021**, *773*, No. 145015.

(43) Sillman, S.; He, D. Some theoretical results concerning O₃-NO_x-VOC chemistry and NO_x-VOC indicators. *J. Geophys. Res.: Atmos.* **2002**, *107*, No. 4659.

(44) Kroll, J. H.; Ng, N. L.; Murphy, S. M.; Flagan, R. C.; Seinfeld, J. H. Secondary organic aerosol formation from isoprene photo-oxidation. *Environ. Sci. Technol.* **2006**, *40*, 1869–1877.

(45) Chen, T.; Liu, J.; Ma, Q.; Chu, B.; Zhang, P.; Ma, J.; Liu, Y.; Zhong, C.; Liu, P.; Wang, Y.; Mu, Y.; He, H. Measurement report: effects of photochemical aging on the formation and evolution of summertime secondary aerosol in Beijing. *Atmos. Chem. Phys.* **2021**, *21*, 1341–1356.

(46) Zhang, S.-H.; Shaw, M.; Seinfeld, J. H.; Flagan, R. C. Photochemical aerosol formation from α -pinene- and β -pinene. *J. Geophys. Res.: Atmos.* **1992**, *97*, 20717–20729.

(47) Wang, Y.; Zhu, S.; Ma, J.; Shen, J.; Wang, P.; Wang, P.; Zhang, H. Enhanced atmospheric oxidation capacity and associated ozone increases during COVID-19 lockdown in the Yangtze River Delta. *Sci. Total Environ.* **2021**, *768*, No. 144796.

(48) Huang, X.; Ding, A.; Gao, J.; Zheng, B.; Zhou, D.; Qi, X.; Tang, R.; Wang, J.; Ren, C.; Nie, W.; Chi, X.; Xu, Z.; Chen, L.; Li, Y.; Che, F.; Pang, N.; Wang, H.; Tong, D.; Qin, W.; Cheng, W.; Liu, W.; Fu, Q.; Liu, B.; Chai, F.; Davis, S. J.; Zhang, Q.; He, K. Enhanced secondary pollution offset reduction of primary emissions during COVID-19 lockdown in China. *Natl. Sci. Rev.* **2021**, *8*, No. nwaal37.

(49) Zhang, X.; Cappa, C. D.; Jathar, S. H.; McVay, R. C.; Ensberg, J. J.; Kleeman, M. J.; Seinfeld, J. H. Influence of vapor wall loss in laboratory chambers on yields of secondary organic aerosol. *Proc. Natl. Acad. Sci. U.S.A.* **2014**, *111*, 5802–5807.

(50) Kroll, J. H.; Seinfeld, J. H. Chemistry of secondary organic aerosol: formation and evolution of low-volatility organics in the atmosphere. *Atmos. Environ.* **2008**, *42*, 3593–3624.

(51) Wood, E. C.; Canagaratna, M. R.; Herndon, S. C.; Onasch, T. B.; Kolb, C. E.; Worsnop, D. R.; Kroll, J. H.; Knighton, W. B.; Seila, R.; Zavala, M.; Molina, L. T.; DeCarlo, P. F.; Jimenez, J. L.; Weinheimer, A. J.; Knapp, D. J.; Jobson, B. T.; Stutz, J.; Kuster, W. C.; Williams, E. J. Investigation of the correlation between odd oxygen and secondary organic aerosol in Mexico City and Houston. *Atmos. Chem. Phys.* **2010**, *10*, 8947–8968.

(52) Iyer, S.; Lopez-Hilfiker, F.; Lee, B. H.; Thornton, J. A.; Kurtén, T. Modeling the Detection of Organic and Inorganic Compounds Using Iodide-Based Chemical Ionization. *J. Phys. Chem. A* **2016**, *120*, 576–587.

(53) Wang, M.; Chen, D.; Xiao, M.; Ye, Q.; Stolzenburg, D.; Hofbauer, V.; Ye, P.; Vogel, A. L.; Mauldin, R. L.; Amorim, A.; Baccarini, A.; Baumgartner, B.; Brilke, S.; Dada, L.; Dias, A.; Duplissy, J.; Finkenzeller, H.; Garmash, O.; He, X.-C.; Hoyle, C. R.; Kim, C.; Kvashnin, A.; Lehtipalo, K.; Fischer, L.; Molteni, U.; Petäjä, T.; Pospisilova, V.; Quéléver, L. L. J.; Rissanen, M.; Simon, M.; Tauber, C.; Tomé, A.; Wagner, A. C.; Weitz, L.; Volkamer, R.; Winkler, P. M.; Kirkby, J.; Worsnop, D. R.; Kulmala, M.; Baltensperger, U.; Dommen, J.; El-Haddad, I.; Donahue, N. M. Photo-oxidation of aromatic hydrocarbons produces low-volatility organic compounds. *Environ. Sci. Technol.* **2020**, *54*, 7911–7921.

(54) Kroll, J. H.; Donahue, N. M.; Jimenez, J. L.; Kessler, S. H.; Canagaratna, M. R.; Wilson, K. R.; Altieri, K. E.; Mazzoleni, L. R.; Wozniak, A. S.; Bluhm, H.; Mysak, E. R.; Smith, J. D.; Kolb, C. E.;

Worsnop, D. R. Carbon oxidation state as a metric for describing the chemistry of atmospheric organic aerosol. *Nat. Chem.* **2011**, *3*, 133–139.

(55) Praske, E.; Otkjaer, R. V.; Crouse, J. D.; Hethcox, J. C.; Stoltz, B. M.; Kjaergaard, H. G.; Wennberg, P. O. Atmospheric autoxidation is increasingly important in urban and suburban North America. *Proc. Natl. Acad. Sci. U.S.A.* **2018**, *115*, 64–69.

(56) Rissanen, M. P. NO₂ Suppression of Autoxidation–Inhibition of Gas-Phase Highly Oxidized Dimer Product Formation. *ACS Earth Space Chem.* **2018**, *2*, 1211–1219.

(57) Bianchi, F.; Kurtén, T.; Riva, M.; Mohr, C.; Rissanen, M. P.; Roldin, P.; Berndt, T.; Crouse, J. D.; Wennberg, P. O.; Mentel, T. F.; Wildt, J.; Junninen, H.; Jokinen, T.; Kulmala, M.; Worsnop, D. R.; Thornton, J. A.; Donahue, N.; Kjaergaard, H. G.; Ehn, M. Highly oxygenated organic molecules (HOM) from gas-phase autoxidation involving peroxy radicals: a key contributor to atmospheric aerosol. *Chem. Rev.* **2019**, *119*, 3472–3509.

(58) Yan, C.; Nie, W.; Vogel, A. L.; Dada, L.; Lehtipalo, K.; Stolzenburg, D.; Wagner, R.; Rissanen, M. P.; Xiao, M.; Ahonen, L.; Fischer, L.; Rose, C.; Bianchi, F.; Gordon, H.; Simon, M.; Heinritzi, M.; Garmash, O.; Roldin, P.; Dias, A.; Ye, P.; Hofbauer, V.; Amorim, A.; Bauer, P. S.; Bergen, A.; Bernhammer, A.-K.; Breitenlechner, M.; Brilke, S.; Buchholz, A.; Mazon, S. B.; Canagaratna, M. R.; Chen, X.; Ding, A.; Dommen, J.; Draper, D. C.; Duplissy, J.; Frege, C.; Heyn, C.; Guida, R.; Hakala, J.; Heikkinen, L.; Hoyle, C. R.; Jokinen, T.; Kangasluoma, J.; Kirkby, J.; Kontkanen, J.; Kürten, A.; Lawler, M. J.; Mai, H.; Mathot, S.; Mauldin, R. L.; Molteni, U.; Nichman, L.; Nieminen, T.; Nowak, J.; Ojdanic, A.; Onnela, A.; Pajunoja, A.; Petäjä, T.; Piel, F.; Quéléver, L. L. J.; Sarnela, N.; Schallhart, S.; Sengupta, K.; Sipilä, M.; Tomé, A.; Tröstl, J.; Väisänen, O.; Wagner, A. C.; Ylisirniö, A.; Zha, Q.; Baltensperger, U.; Carslaw, K. S.; Curtius, J.; Flagan, R. C.; Hansel, A.; Riipinen, I.; Smith, J. N.; Virtanen, A.; Winkler, P. M.; Donahue, N. M.; Kerminen, V.-M.; Kulmala, M.; Ehn, M.; Worsnop, D. R. Size-dependent influence of NO_x on the growth rates of organic aerosol particles. *Sci. Adv.* **2020**, *6*, No. eaay4945.

(59) Wang, Y.; Clusius, P.; Yan, C.; Dallenbach, K.; Yin, R.; Wang, M.; He, X. C.; Chu, B.; Lu, Y.; Dada, L.; Kangasluoma, J.; Rantala, P.; Deng, C.; Lin, Z.; Wang, W.; Yao, L.; Fan, X.; Du, W.; Cai, J.; Heikkinen, L.; Tham, Y. J.; Zha, Q.; Ling, Z.; Junninen, H.; Petaja, T.; Ge, M.; Wang, Y.; He, H.; Worsnop, D. R.; Kerminen, V. M.; Bianchi, F.; Wang, L.; Jiang, J.; Liu, Y.; Boy, M.; Ehn, M.; Donahue, N. M.; Kulmala, M. Molecular composition of oxygenated organic molecules and their contributions to organic aerosol in Beijing. *Environ. Sci. Technol.* **2022**, *56*, 770–778.

(60) Farmer, D. K.; Matsunaga, A.; Docherty, K. S.; Surratt, J. D.; Seinfeld, J. H.; Ziemann, P. J.; Jimenez, J. L. Response of an aerosol mass spectrometer to organonitrates and organosulfates and implications for atmospheric chemistry. *Proc. Natl. Acad. Sci. U.S.A.* **2010**, *107*, 6670–6675.

(61) Gao, Q.; Yan, Y.; Li, R.; Xu, Y.; Niu, Y.; Liu, C.; Xie, K.; Chang, Z.; Hu, D.; Li, Z.; Peng, L. Characteristics of Volatile Organic Compounds during Different Pollution Periods in Winter in Yuncheng, a Typical City in North China. *Aerosol Air Qual. Res.* **2020**, *20*, 97–107.

(62) Han, L.; Chen, L.; Li, K.; Bao, Z.; Zhao, Y.; Zhang, X.; Azzi, M.; Cen, K. Source Apportionment of Volatile Organic Compounds (VOCs) during Ozone Polluted Days in Hangzhou, China. *Atmosphere* **2019**, *10*, No. 780.

(63) He, H.; Wang, Y.; Ma, Q.; Ma, J.; Chu, B.; Ji, D.; Tang, G.; Liu, C.; Zhang, H.; Hao, J. Mineral dust and NO_x promote the conversion of SO₂ to sulfate in heavy pollution days. *Sci. Rep.* **2014**, *4*, No. 04172.

(64) Ma, J.; Chu, B.; Liu, J.; Liu, Y.; Zhang, H.; He, H. NO_x promotion of SO₂ conversion to sulfate: an important mechanism for the occurrence of heavy haze during winter in Beijing. *Environ. Pollut.* **2018**, *233*, 662–669.

(65) Chu, B.; Zhang, S.; Liu, J.; Ma, Q.; He, H. Significant concurrent decrease in PM_{2.5} and NO₂ concentrations in China during COVID-19 epidemic. *J. Environ. Sci.* **2021**, *99*, 346–353.

(66) Chu, B.; Ma, Q.; Liu, J.; Ma, J.; Zhang, P.; Chen, T.; Feng, Q.; Wang, C.; Yang, N.; Ma, H.; Ma, J.; Russell, A. G.; He, H. Air Pollutant Correlations in China: Secondary Air Pollutant Responses to NO_x and SO₂ Control. *Environ. Sci. Technol. Lett.* **2020**, *7*, 695–700.

(67) Chu, B.; Ding, Y.; Gao, X.; Li, J.; Zhu, T.; Yu, Y.; He, H. Coordinated control of fine-particle and ozone pollution by the substantial reduction of nitrogen oxides. *Engineering* **2021**, DOI: 10.1016/j.eng.2021.09.006.